ARTICLE

OBC
www.rsc.org/obc

Theoretical (DFT, GIAO–NMR, NICS) study of carbocations $(M+H)^+$, dications (M^{2+}) and dianions (M^{2-}) from dihydro-dicyclopenta[*ef*,*kl*]heptalene (dihydro-azupyrene), dihydro-dicyclohepta[*ed*,*gh*]pentalene, and related bridged [14]annulenes†

Takao Okazaki[a,b] **and Kenneth K. Laali***[b]

[a] *Department of Energy and Hydrocarbon Chemistry, Kyoto University, Kyoto, Japan*
[b] *Department of Chemistry, Kent State University, Kent, OH 44242, USA. E-mail: klaali@kent.edu; Fax: 330-6723816; Tel: 330-6722988*

Received 5th August 2004, Accepted 11th September 2004
First published as an Advance Article on the web 13th December 2004

The annulenium ions of protonation, the two-electron oxidation dications, and the two-electron reduction dianions derived from dihydro- and dimethyldihydro derivatives (*cis* and *trans*) of dicyclopenta[*ef*,*kl*]heptalene (azupyrene) (**1**) and dicyclohepta[*ed*,*gh*]pentalene (**2**), which are the nonalternant isomers of pyrene, were studied by density functional theory (DFT) at the B3LYP/6-31G(d), 6-31+G(d,p), or 6–31++G(d,p) levels. Charge delocalization modes in the energetically most favored annulenium ions, as well as in the singlet and triplet dications and dianions, were assessed based on gauge-including atomic orbital (GIAO) $\Delta\delta^{13}$C values and *via* changes in natural population analysis (NPA) charges. Relative aromaticity/antiaromaticity in the annulenes were gauged *via* nucleus-independent chemical shift (NICS) and ΔNICS. Annulenium ions of monoprotonation, the dications, and dianions derived from bismethano- and propanediylidene [14]annulenes were also studied by DFT for comparison with the *cis*-dihydro isomers derived from **2**. Computed GIAO NMR data and the optimized geometries were compared with the experimental data when available, and the optimized geometries were compared with the X-ray data if known. A basis-set dependency study of the computed GIAO chemical shifts was also undertaken. The present DFT work represents the first detailed comparative theoretical study of charged annulenes derived from the dihydro derivatives of **1** and **2**.

Introduction

Dicyclopenta[*ef*,*kl*]heptalene, DCPH or "azupyrene" (**1**) and dicyclohepta[*ed*,*gh*]pentalene, (DCHP, **2**), Fig. 1, are the non-alternant isomers of pyrene **3**. They constitute 14π-Hückel aromatic peripheral systems perturbed by a central double bond. The X-ray structures of **1–2** are available,[1,2] but knowledge concerning their chemical properties is still quite limited and bioactivity data are as yet nonexistent.[3–7] Moreover, only limited data are available on the electronic structures, NMR characteristics and relative aromaticity/antiaromaticity in their carbocations, dications and dianions. A recent DFT study[8] focused on the mono- and diprotonation carbocations and the oxidation dications derived from **1–3**.

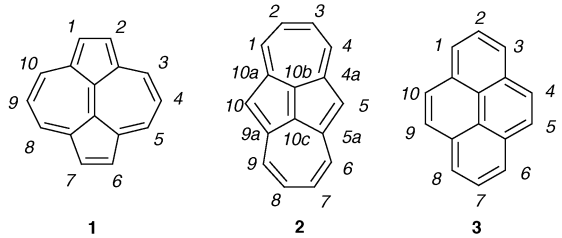

Fig. 1 Dicyclopenta[*ef*,*kl*]heptalene (**1**), dicyclohepta[*ed*,*gh*]pentalene (**2**), and pyrene (**3**).

Focusing on the corresponding *trans*- as well as *cis*-dihydro derivatives **4–13** (Fig. 2), Boekelheide's *trans*-15,16-dimethyldihydropyrene (DMDHP, **13**),[9] is a well studied planar bridged 14π-diatropic annulene, the shielded internal methyl groups of which proved to be an excellent probe of the ring-current effects and aromaticity in annulenes.[10–13] Numerous carbocyclic ring-fused and benzannelated derivatives of **13** have been synthesized in order to gauge changes in diatropicity due to bond localization. The 16π paratropic dianion ($\mathbf{13}^{2-}$) and several persistent 12π-annulenium ions ($\mathbf{13H}^+$) have been generated and studied by NMR.[14,15] In addition, a number of stable carboxonium–annulenium dications have been prepared from the cyclohexenone- and cyclopentenone-fused derivatives of **13**,[16] and more recently, examples of diprotonated dications have been reported starting from the di- and tetramethyl derivatives of **13**.[17] DFT studies on parent **13** and some of

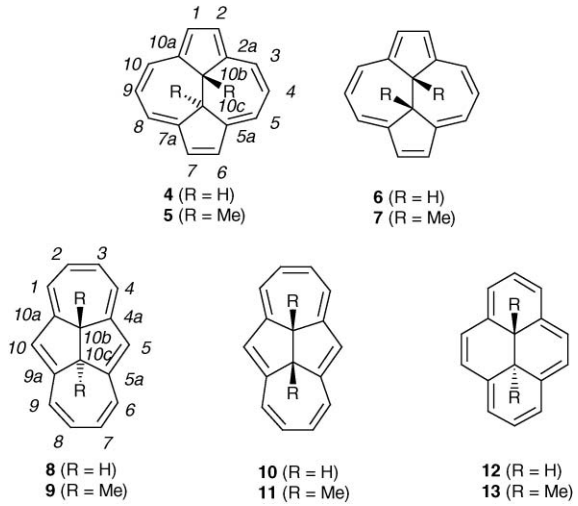

Fig. 2 Dihydro derivatives of **1–3**.

† Electronic supplementary information (ESI) available: DFT calculations, reported X-ray structures, NMR chemical shifts, NPA-derived charges, NICS and ΔNICS values, experimental δ^{13}C, δ^{1}H, HOMO, LUMO, and SOMO. See http://www.rsc.org/suppdata/ob/b4/b412043d/

DOI: 10.1039/b412043d

its ring-fused derivatives,[18] and limited theoretical studies on dimethyldihydropyrenium cations (**13**H$^+$) have been reported.[15]

In comparison to extensive studies on *trans*-DMDHP and its derivatives, the dihydro derivatives of azupyrene (as in **4** and **5**, *anti*; and **6** and **7**, *syn*) have not received much attention. Synthetic access to *trans*-dialkyl-dihydro compounds is possible according to Müllen and associates[19] *via* nucleophilic addition to the central double bond of **1**, followed by quenching of the resulting monoanions with typical electrophiles which produced a series of *trans*-dialkyl substituted derivatives of **4**. The ^{1}H NMR spectrum of **5** has been reported with the internal methyls appearing at −4.53 ppm.[20] The internal methyls in the 16π-paratropic dianion **5**$^{2-}$, formed by reduction with potassium metal, appear at 11.96 ppm in the ^{1}H NMR.[21] It was reported earlier that reduction of **5** gave the C_4/C_9 dihydro derivative.[21]

As for the dihydro derivative of **2**, whereas the *trans*-isomers **8** and **9** are the nonalternant analogs of **12** and **13**, the *cis*-isomers (**10**, **11**) belong to the family of bridged [14]annulenes with an anthracene perimeter, whose syntheses were reported by Vogel *et al.*[5] (although *syn*/*anti* designations may be more suitable for the dihydro derivatives, the *cis*/*trans* designations commonly used for DMDHP and its derivatives are adopted here). The ring protonated annulenium ion of **10** as well as those of the related bridged [14]annulenes **14** (bismethano-) and **15** (propanediylidene-) (Fig. 3) were reported by Michl and associates.[22] NMR data are also available on persistent dications and dianions of these annulenes.[20,21]

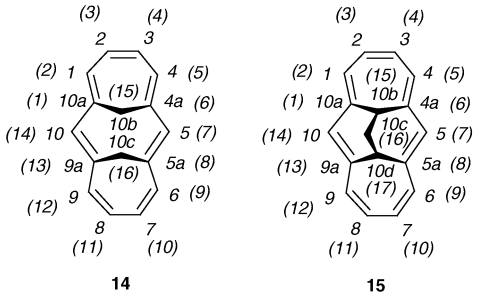

Fig. 3 Studied bridged [14]annulenes (carbon numbering system adopted is for comparison with hydrocarbons **4**–**11**; carbon numbering system according to Vogel *et al.* in parentheses).

We report here a DFT study on the dihydro azupyrenes **4** and **5**, and dihydro dicyclohepta[*ed*,*gh*]pentalenes (**8**–**11**) (see Fig. 2), focusing on their annulenium ions of protonation, two-electron oxidation dications, and two-electron reduction dianions. For comparison, the carbocations, dications and dianions derived from **14** and **15** were also studied by DFT. The geometrical features, GIAO-NMR chemical shifts and NICS in the preferred annulenium ions, annulene dications and dianions, are compared with their neutral annulene precursors in order to elucidate charge delocalization modes in the resulting annulenes (gauged *via* $\Delta\delta^{13}$C values by GIAO-NMR and the NPA-derived changes in charges) and relative aromaticity/antiaromaticity in various rings (gauged *via* NICS and ΔNICS). The GIAO-NMR data are compared with the experimental values when known.

Results and discussion

DFT calculations

Structures were optimized using molecular point groups (shown in Tables S1–4 of the electronic supplementary information†) by the density functional theory (DFT) method at B3LYP/6-31G(d), 6-31+G(d,p), or 6-31++G(d,p) level using the Gaussian 03 package.[23] Singlet and triplet states were treated with restricted (ROB3LYP) and unrestricted (UB3LYP) approach, respectively. Computed geometries were verified by frequency calculations. Furthermore, global minima were checked by manually changing initial geometries and by comparing the resulting optimized structures and their energies. NMR chemical shifts and NICS[24] (nucleus-independent chemical shift) values were calculated by the GIAO[25] (gauge-including atomic orbital) method at the B3LYP/6-31G(d)//B3LYP/6-31G(d) level. In cases where experimental ^{13}C NMR chemical shifts were available (**10a**H$^+$, **14**H$^+$, singlet **14**$^{2+}$, singlet **14**$^{2-}$, **15**H$^+$, and singlet **15**$^{2+}$), basis-set dependency studies of GIAO chemical shifts were performed with the GIAO-derived δ^{13}C at B3LYP/6-31G(d)//B3LYP/6-31G(d), B3LYP/6-31+G(d,p)//B3LYP/6-31G(d), B3LYP/6-311++G(d,p)//B3LYP/6-31G(d), B3LYP/6-311++G(3df,3pd)//B3LYP/6-31G(d), and B3LYP/6-311++G(d,p)//B3LYP/6-311++G(d,p) levels. For comparison in selected cases, optimized geometries, relative energies, ^{13}C NMR chemical shifts, the natural population analysis (NPA)-derived charges, and NICS values were computed at the B3LYP/6-31+G(d,p) and B3LYP/6-31++G(d,p) levels. NMR chemical shifts were referenced to TMS [GIAO magnetic shielding tensor = 189.7717 ppm at the B3LYP/6-31G(d) level, 192.5643 ppm at the B3LYP/6-31+G(d,p) level, and 192.5776 ppm at the B3LYP/6-31++G(d,p) level; this value is related to the GIAO isotropic magnetic susceptibility for ^{13}C], calculated with a molecular symmetry of T_d at the same level of theory. NICS values were computed at zero angstroms above the ring centroid which was defined as the simple average of Cartesian coordinates for all carbons (sp^2 and sp^3) in the inner ring and over all the rings. Tables S1–4 (supplementary information†) summarize the total energies (*E*), zero point energies (*ZPE*), Gibbs free energies (*G*), and Gibbs free energies relative to those of the parent hydrocarbons (Δ*G*) for the neutral substrates, the protonated carbocations, the oxidation dications, and the reduction dianions. Gibbs free energies were evaluated by frequency calculations at 298 K under 1 atm pressure which is the default for the Gaussian 03 program.

On the relative stabilities of the dihydro derivatives

According to DFT, whereas the *trans*-dihydro-azupyrenes **4** and **5** are more stable than the corresponding *cis*-isomers **6** and **7**, the opposite relative stability trend is observed for the dihydro-dicyclohepta[*ed*,*gh*]pentalenes (**8**–**11**), where the *cis*-isomers are considerably more stable (Table S1, supplementary information†).

Protonation, oxidation and reduction of *trans*-10*b*,10*c*-dihydrodicyclopenta[*ef*,*kl*]heptalene (4)

DFT-optimized structures of **4** (C_1 symmetry), **4**H$^+$ (C_1), **4a**H$^+$ (C_1), **4b**H$^+$ (C_1), the triplet dication **4**$^{2+}$ (C_1), and the singlet dianion **4**$^{2-}$ (C_1) were calculated to be minima (Fig. 4 and 5, Fig. S1–2, Table S2; supplementary information†). These geometries are almost the same as the C_{2h} symmetrical structure for **4**, triplet **4**$^{2+}$, and singlet **4**$^{2-}$, and the C_2 for **4b**H$^+$.

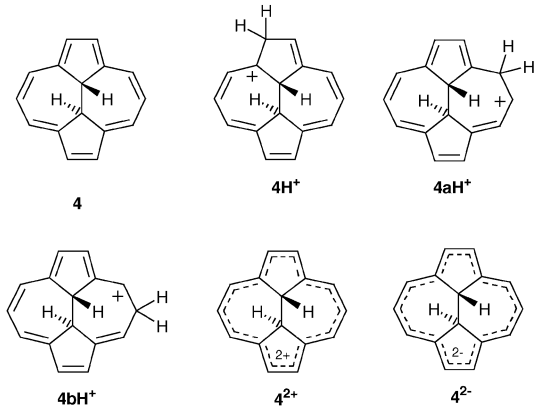

Fig. 4 *trans*-10*b*,10*c*-Dihydrodicyclopenta[*ef*,*kl*]heptalene (**4**), protonated *trans*-10*b*,10*c*-dihydrodicyclopenta[*ef*,*kl*]heptalenium ions (**4**H$^+$, **4a**H$^+$, and **4b**H$^+$), the dication (**4**$^{2+}$), and the dianion (**4**$^{2-}$).

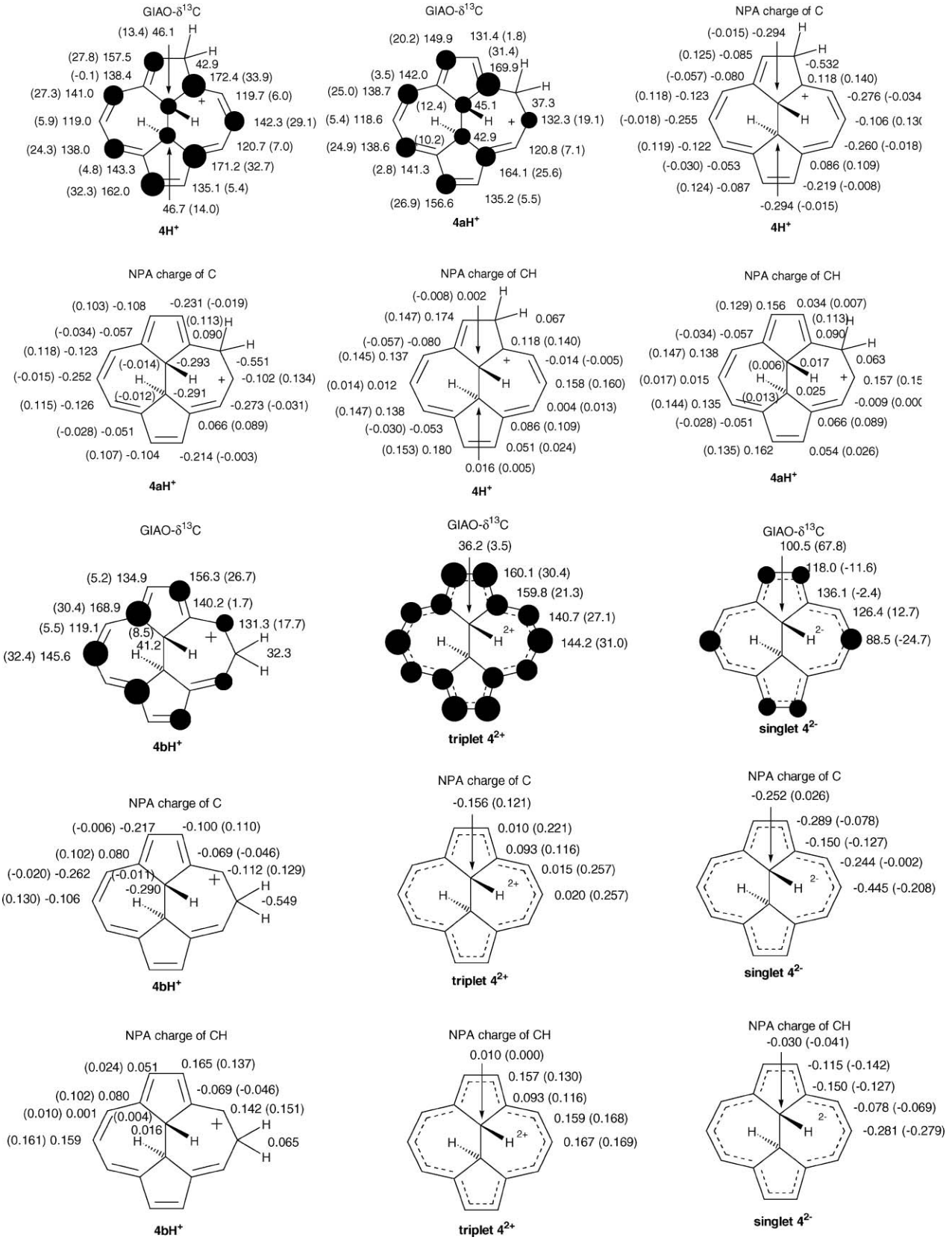

Fig. 5 Computed ^{13}C NMR chemical shifts, NPA-derived carbon charges, and NPA-derived overall charges over CH units for **4**H$^+$, **4a**H$^+$, **4b**H$^+$, **4**$^{2+}$, and **4**$^{2-}$ ($\Delta\delta$ ^{13}Cs and Δ charges relative to **4** in parentheses). [Dark circles are roughly proportional to the magnitude of $\Delta\delta$ ^{13}Cs (positive/downfield for the carbocations/dication and negative/upfield for the dianion); threshold was set to 10 ppm].

Relative energies of the [12]annulenium ions derived from **4** are in close range, with **4b**H$^+$ (C-4 protonated) being most preferred, followed closely by **4a**H$^+$ (C-3 protonated, 2.6 kcal mol^{-1} higher) and **4**H$^+$ (C-1 protonated, <1 kcal mol^{-1} higher).

Whereas the triplet dication **4**$^{2+}$ is slightly more stable than the singlet **4**$^{2+}$ (by *ca.* 1.2 kcal mol^{-1}), the opposite is true for the dianion **4**$^{2-}$, where the singlet state was computed to be more stable than the triplet state by *ca.*1.7 kcal mol^{-1}.

The central bond and the four inner connecting bonds in parent **4** are noticeably long, relative to the peripheral bonds. The central and the inner bonds remain long in the carbocations and are in many cases longer than the sp^3–sp^2 bonds resulting

from protonation. Clear bond alternation (long/short) patterns are observed in the peripheral bonds in the [12]annulenium ions derived from **4**. The peripheral bonds in triplet $\mathbf{4}^{2+}$ are longer than in parent **4**. The C_1–C_2 bond (5-membered ring) in singlet $\mathbf{4}^{2-}$ is noticeably short and there is a clear bond-alternation pattern at the periphery (see supplementary information†, Fig. S1).

Forms of the HOMO–LUMO for **4**, $\mathbf{4b}H^+$, singlet $\mathbf{4}^{2+}$, singlet $\mathbf{4}^{2-}$, and SOMOs for triplet $\mathbf{4}^{2+}$ and $\mathbf{4}^{2-}$ (computed at the B3LYP/6-31G(d) level) are collected in Fig. S25 for comparison (supplementary information†). Variations in the computed bond lengths upon oxidation and reduction in these systems appear to correlate with the forms of HOMO–LUMO. The HOMO of singlet $\mathbf{4}^{2-}$ and the LUMO of **4** are similar (singlet $\mathbf{4}^{2-}$ is formed by adding two electrons to the LUMO of **4**). For singlet $\mathbf{4}^{2-}$, the C_1–C_2 and C_6–C_7 bonds with π-bonding in HOMO were calculated to be shorter than those of **4** in the optimized geometry. It can be considered that the triplet $\mathbf{4}^{2+}$ is generated by removal of one electron from HOMO and one electron from HOMO-1 in **4** (this gives rise to SOMOs of the dication). In this case, the C–C bonds (C_1–C_2, C_2–C_{2a}, C_{2a}–C_3, C_5–C_{5a}, C_{5a}–C_6, C_6–C_7, C_7–C_{7a}, C_{7a}–C_8, C_{10}–C_{10a}, and C_{10a}–C_1) with π-bonding orbitals in SOMOs become longer.

Charge delocalization modes deduced based on magnitude of GIAO $\Delta\delta^{13}$C values in the monocation $\mathbf{4}H^+$, $\mathbf{4a}H^+$, $\mathbf{4b}H^+$, triplet dication $\mathbf{4}^{2+}$, and singlet dianion $\mathbf{4}^{2-}$ are sketched in Fig. 5 for comparison. The NPA-derived carbon and CH charges and changes in charges are also included.

Positive charge in the monocations $\mathbf{4}H^+$, $\mathbf{4a}H^+$, $\mathbf{4b}H^+$ is extensively delocalized, residing at the alternating carbons over the periphery. Whereas the charge delocalization pattern for $\mathbf{4}H^+$ and $\mathbf{4a}H^+$ are similar, that for $\mathbf{4b}H^+$ is opposite. The NPA-derived changes in charges create analogous charge patterns and are overall in good agreement with the GIAO $\Delta\delta^{13}$C-based conclusions. The positive charge in triplet $\mathbf{4}^{2+}$ is delocalized throughout the periphery and exists on all carbons with the C_1/C_2 and C_4/C_9 bearing the largest $\Delta\delta^{13}$C values. Based on both the GIAO $\Delta\delta^{13}$C and the computed NPA changes in charges, the C_4/C_9 positions are logical candidates for electrophilic attack on singlet $\mathbf{4}^{2-}$ and this prediction is in concert with experimental outcome (formation of C_4/C_9 dihydro derivative upon reduction).[21]

The computed NICS(0) and ΔNICS values for the [12]annulenium ions $\mathbf{4}H^+$, $\mathbf{4a}H^+$, $\mathbf{4b}H^+$, the [14]annulene dication $\mathbf{4}^{2+}$ and the [16]annulene dianion $\mathbf{4}^{2-}$ are gathered in Fig. S2 for comparison (supplementary information†). The 5-membered rings in $\mathbf{4a}H^+$ are aromatic, that in $\mathbf{4b}H^+$ is borderline aromatic, whereas other rings are non-aromatic. For $\mathbf{4}^{2+}$ and $\mathbf{4}^{2-}$ (both representing 4nπ antiaromatic/paratropic systems), NICS(0) measured at the center of the molecules suggests that the singlet $\mathbf{4}^{2+}$ is antiaromatic and the singlet $\mathbf{4}^{2-}$ is nonaromatic. By contrast, NICS values (gauged at center) for triplet $\mathbf{4}^{2+}$ and triplet $\mathbf{4}^{2-}$ are highly negative and imply strong aromatic character! It should be noted, however, that NICS(0)s measured at the center of the molecules are shielded by electrons of the central C–C bonds, since their locations are in the bonds. Therefore, real NICS values could be more positive than computed.

In order to assess the influence of basis set on relative energies, optimized geometries, as well as on the GIAO chemical shifts and NICS, the carbocations, singlet dications and the singlet and triplet dianions derived from azupyrene **4** were re-examined by DFT at the B3LYP/6-31+G(d,p) and B3LYP/6-31++G(d,p) levels. The data are gathered in Table S3 and in Fig. S1a–S1c and Fig. S2 (supplementary information†). It is apparent that inclusion of diffuse functions in the basis sets has little impact on the optimized geometries and the GIAO shifts, and the comparative aspects remain unchanged. But, as Table S3 illustrates, relative energies are lowered in many cases (see also further discussion and Table S4; supplementary information†). This is especially true for the singlet and triplet dianions. Nevertheless, relative stability order of triplet $\mathbf{4}^{2+}$ > singlet $\mathbf{4}^{2+}$ and singlet $\mathbf{4}^{2-}$ > triplet $\mathbf{4}^{2-}$ remains unchanged, except at the B3LYP/6-31++G(d,p) level where triplet $\mathbf{4}^{2-}$ became more stable than singlet $\mathbf{4}^{2-}$ (several attempts were made to optimize the structure of triplet $\mathbf{4}^{2-}$ at the B3LYP/6-31++G(d,p) level by changing its initial geometry, however, frequency calculations showed one imaginary frequency).

As far as NICS is concerned, basis set dependency is well documented,[24b] and is clearly evident here (see Fig. S2, supplementary information†). As was pointed out before,[24b] comparisons must only be made at the same calculational levels. It may be surmised that, based on NICS(0), whereas singlet $\mathbf{4}^{2+}$ and singlet $\mathbf{4}^{2-}$ exhibit antiaromatic character, the corresponding triplet dications are aromatic. The NICS-derived argument ties in with the computed relative stability order for $\mathbf{4}^{2+}$ (triplet lower than singlet) but not necessarily with $\mathbf{4}^{2-}$ (singlet lower than triplet!—see also comparative discussion).

Protonation, oxidation and reduction of *trans*-10*b*,10*c*-dimethyl-10*b*,10*c*-dihydrodicyclopenta[*ef*,*kl*]heptalene (5)

Compound **5** is the nonalternant analog of DMDHP. DFT-optimized structures of **5** (C_1 symmetry), $\mathbf{5}H^+$ (C_1), $\mathbf{5a}H^+$ (C_1), $\mathbf{5b}H^+$ (C_1), the triplet dication $\mathbf{5}^{2+}$ (C_i), the singlet dication $\mathbf{5}^{2+}$ (C_1), and the singlet dianion $\mathbf{5}^{2-}$ (C_1) were calculated to be minima (Fig. S3 and Table S2, supplementary information†). These geometries are almost the same as the C_{2h} symmetrical structure for **5**, singlet $\mathbf{5}^{2+}$, and singlet $\mathbf{5}^{2-}$, and the C_2 for $\mathbf{5b}H^+$.

A noteworthy feature in the optimized geometries of annulenes **4** and **5** is that the central bond (C_{10b}–C_{10c}) in **5** is much longer, whereas other bond lengths are rather close. Overall, the geometrical features for the monoprotonated annulenium ions, the dication and the dianion derived from the *trans*-dimethyl derivative **5** *versus* those derived from the *trans*-dihydro derivative **4** are rather similar. The C_1–C_2 bond in $\mathbf{5b}H^+$ is noticeably short, and the singlet $\mathbf{5}^{2-}$ and $\mathbf{4}^{2-}$ have the longest central bonds (1.629 and 1.618 Å).

The outcome of monoprotonation of **5** (Fig. 6 and Table 2, supplementary information†) is the same as that for **4**, with the annulenium ion $\mathbf{5b}H^+$ (protonated at C-4) favored by 2 kcal mol^{-1} over the carbocations of attack at C-1 and C-3 which have nearly identical energies. Whereas the dication $\mathbf{5}^{2+}$ is predicted to be degenerate (nearly the same energy for the singlet and triplet), the singlet dianion $\mathbf{5}^{2-}$ is computed to be more stable than the triplet (the NMR spectrum of $\mathbf{5}^{2-}$ has been reported in ref. 21).

Charge delocalization modes deduced based on magnitude of GIAO $\Delta\delta^{13}$C values and the NPA changes in charges in monocations, dication and dianion derived from **5** are sketched in Fig. S4 for comparison (supplementary information†). These patterns are very similar to those predicted for **4**. The sites of

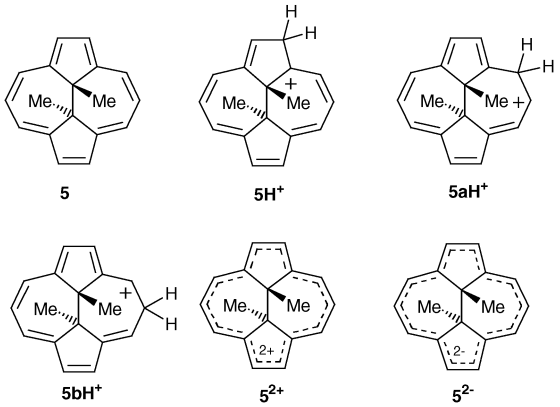

Fig. 6 *trans*-10*b*,10*c*-Dimethyl-10*b*,10*c*-dihydrodicyclopenta[*ef*,*kl*]heptalene (**5**), its protonated annulenium ions ($\mathbf{5}H^+$, $\mathbf{5a}H^+$, and $\mathbf{5b}H^+$), the dication ($\mathbf{5}^{2+}$), and the dianion ($\mathbf{5}^{2-}$).

electrophilic attack on $\mathbf{5}^{2-}$ are similarly predicted to be C_4/C_9 (in line with experiment). The computed NICS and ΔNICS values (Fig. S5, supplementary information†) for the annulenium ions derived from **5** are similar to those of **4**, with the 5-membered rings computed to be aromatic. Whereas NICS values measured at the center of singlet $\mathbf{5}^{2+}$ and singlet $\mathbf{5}^{2-}$ imply antiaromaticity, for triplet $\mathbf{5}^{2+}$ and $\mathbf{5}^{2-}$ highly negative NICS values are computed which are indicative of strong aromatic character. In the case of singlet and triplet $\mathbf{5}^{2-}$, NICS values were also computed at higher level (see Fig. S5, supplementary information†).

Annulene ions derived from *trans*-10*b*,10*c*-dihydrodicyclohepta-[*ed*,*gh*]pentalene (8)

Structures of **8** (C_1), protonated annulenium ions $\mathbf{8}H^+$, $\mathbf{8a}H^+$, $\mathbf{8b}H^+$ (all C_1), the singlet and triplet $\mathbf{8}^{2+}$ (C_1) and $\mathbf{8}^{2-}$ (C_1) were found to be minima by DFT. These geometries are almost the same as the C_{2h} symmetrical structure for **8**, $\mathbf{8}^{2+}$, and $\mathbf{8}^{2-}$, and C_2 for $\mathbf{8}H^+$ (Table S2 (supplementary information†) and Fig. 7). Protonation at the 5-membered ring ($\mathbf{8}H^+$) is most favored followed closely by C-2 protonation ($\mathbf{8a}H^+$). The least favored annulenium ion ($\mathbf{8b}H^+$) lies 4 kcal mol^{-1} higher than $\mathbf{8}H^+$. The singlet states of $\mathbf{8}^{2+}$ and $\mathbf{8}^{2-}$ are preferred over their corresponding triplet states.

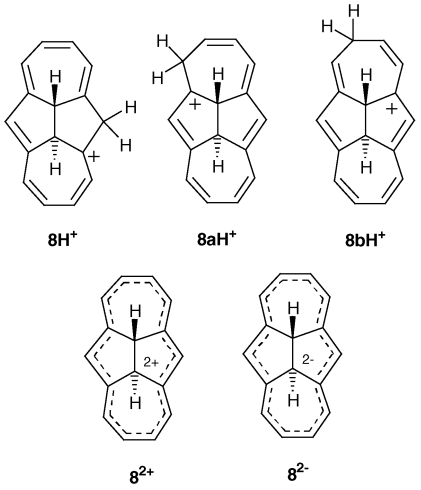

Fig. 7 *trans*-10*b*,10*c*-Dihydrodicyclohepta[*ed*,*gh*]pentalene (**8**), annulenium ions ($\mathbf{8}H^+$, $\mathbf{8a}H^+$, and $\mathbf{8b}H^+$), dication ($\mathbf{8}^{2+}$), and dianion ($\mathbf{8}^{2-}$).

Charge delocalization modes deduced based on magnitude of GIAO $\Delta\delta^{13}C$ values in the energetically most preferred monocation $\mathbf{8}H^+$, singlet dications $\mathbf{8}^{2+}$, and singlet dianion $\mathbf{8}^{2-}$ are sketched in Fig. 8 for comparison. The NPA-derived carbon and CH charges and changes in charges are also included. Positive charge in $\mathbf{8}H^+$ is highly delocalized and alternates at the periphery of the annulenium ion. The C_{10b}/C_{10c} carbons (central bond) are also positive. Positive charge in the singlet $\mathbf{8}^{2+}$ is more strongly localized on the 5-membered rings. The negative charge in singlet $\mathbf{8}^{2-}$ is mainly localized on C_5/C_{10} and C_1/C_4, and these sites are most appropriate for subsequent electrophilic addition. The overall charge delocalization patterns deduced based on changes in computed NPA charges agree with the GIAO-derived patterns.

Relative to parent **8**, the central bonds in the $\mathbf{8}^{2-}$, $\mathbf{8}^{2+}$ and $\mathbf{8}H^+$ are noticeably longer and the optimized geometries (Fig. S6, supplementary information†) support peripheral bond-alternation (long/short)

The computed NICS and ΔNICS values for the dication and dianion are gathered in Fig. S7 (supplementary information†). For $\mathbf{8}H^+$, the 5-membered ring is aromatic and the 7-membered rings are antiaromatic. Whereas the singlets $\mathbf{8}^{2+}$ and $\mathbf{8}^{2-}$ are predicted to be strongly antiaromatic, strong aromatic character is predicted for the triplet $\mathbf{8}^{2+}$ and $\mathbf{8}^{2-}$, both in their individual rings and in the center of the annulenes. NICS values computed at higher basis set for the singlet and triplet $\mathbf{8}^{2-}$ lead to a similar conclusion.

Annulene ions derived from *trans*-10*b*,10*c*-dimethyl-10*b*,10*c*-dihydrodicyclohepta[*ed*,*gh*]pentalene (9)

DFT-optimized structures of **9** (C_1), $\mathbf{9}H^+$, $\mathbf{9a}H^+$, $\mathbf{9b}H^+$ (all C_1), $\mathbf{9}^{2+}$ (C_1), and $\mathbf{9}^{2-}$ (C_1) were found to be minima. These geometries are almost the same as the C_{2h} symmetrical structure for **9**, $\mathbf{9}^{2+}$, and $\mathbf{9}^{2-}$, and the C_2 for $\mathbf{9}H^+$. Among three possible annulenium ions of mono-protonation (see Fig. 9), $\mathbf{9}H^+$ (attack at C-5) is strongly preferred, and singlet $\mathbf{9}^{2+}$ and singlet $\mathbf{9}^{2-}$ are more stable than the triplet states.

Charge delocalization modes deduced based on magnitude of GIAO $\Delta\delta^{13}C$ values and the changes in NPA charges in the monocation $\mathbf{9}H^+$, singlet $\mathbf{9}^{2+}$, and singlet dianion $\mathbf{9}^{2-}$ (sketched in Fig. S8 for comparison; supplementary information†) are essentially the same as those deduced for the annulene ions of **8**. The optimized geometries for **9** and its ions are sketched in Fig. S9 for comparison (supplementary information†). The central bond in the dimethyl derivative **9** is noticeably longer than that in the dihydro derivative **8**. Further lengthening of this bond occurs in $\mathbf{9}H^+$, $\mathbf{9}^{2+}$, and $\mathbf{9}^{2-}$ for which the peripheral bond lengths clearly support regular bond-alternation.

The computed NICS and ΔNICS values for these cations (sketched in Fig. S10, supplementary information†) reflect the same patterns as those discussed for **8**.

Annulene ions from *cis*-10*b*,10*c*-dihydrodicyclohepta[*ed*,*gh*]-pentalenes (10 and 11)

Reel and Vogel[5] synthesized compound **2** from **10** by hydride abstraction with trityl salt followed by quenching with water. An open question was whether $\mathbf{2a}H^+$ (see Fig. 10) is the direct precursor to **2** or if a rapid rearrangement to $\mathbf{2b}H^+$ ensued and the latter was the primary precursor to **2**. In the context of the present DFT study, we have computed the relative energies of these carbocations and found that $\mathbf{2b}H^+$ is 17.1 kcal mol^{-1} more stable than $\mathbf{2a}H^+$. It can be surmised, then, that the initially formed hydride abstraction cation rapidly rearranges ($\mathbf{2a}H^+ \rightarrow \mathbf{2b}H^+$), and that $\mathbf{2b}H^+$ is most likely the main precursor to **2**.

Structures of $\mathbf{10}H^+$, $\mathbf{10a}H^+$, and $\mathbf{10b}H^+$ (all C_1), singlet $\mathbf{10}^{2+}$ (C_1), and the singlet dianion $\mathbf{10}^{2-}$ (C_1) were computed by DFT to be minima (Fig. 11 and Table S2; supplementary information†). These geometries are almost the same as the C_{2v} symmetrical structure for **10**, $\mathbf{10}^{2+}$, and $\mathbf{10}^{2-}$. Similarly, structures of **11** (C_1), $\mathbf{11a}H^+$ (C_1), $\mathbf{11b}H^+$ (C_1), the singlet dication $\mathbf{11}^{2+-}$ (C_1), and the singlet dianion $\mathbf{11}^{2-}$ (C_1) were calculated to be minima (Fig. 12 and Table S2; supplementary information†).

Comparison between the optimized structures of **8** *versus* **10** and **9** *versus* **11** is instructive (Fig. S6, S9, S11, S12; supplementary information†). The central bonds in the *cis*-isomers (**10** and **11**) are considerably longer than those in the *trans*-isomers (**8** and **10**) and there is a greater degree of bond alternation at the periphery in the *trans*-isomers compared to *cis*.

The X-ray structure of **11** has been reported in the literature.[26] (in Fig. S12, supplementary information†), but no data for **10** have been reported. The computed bond lengths are somewhat longer than those from X-ray structure. The same feature was recently noted for **1**[8] (shorter X-ray derived bonds relative to DFT at B3LYP/6-31G(d) and at B3LYP/6-311++G(d,p) levels with improved match at the HF/6-31G(d) level).

Whereas no persistent carbocations from **8** or **9** are reported, low temperature protonation of **10** gave $\mathbf{10a}H^+$ as a persistent carbocation.[22] Among the monoprotonated annulenium ions derived from **10**, $\mathbf{10a}H^+$ is computed to be most favored, and this agrees with the earlier reported NMR study.[22] Similarly,

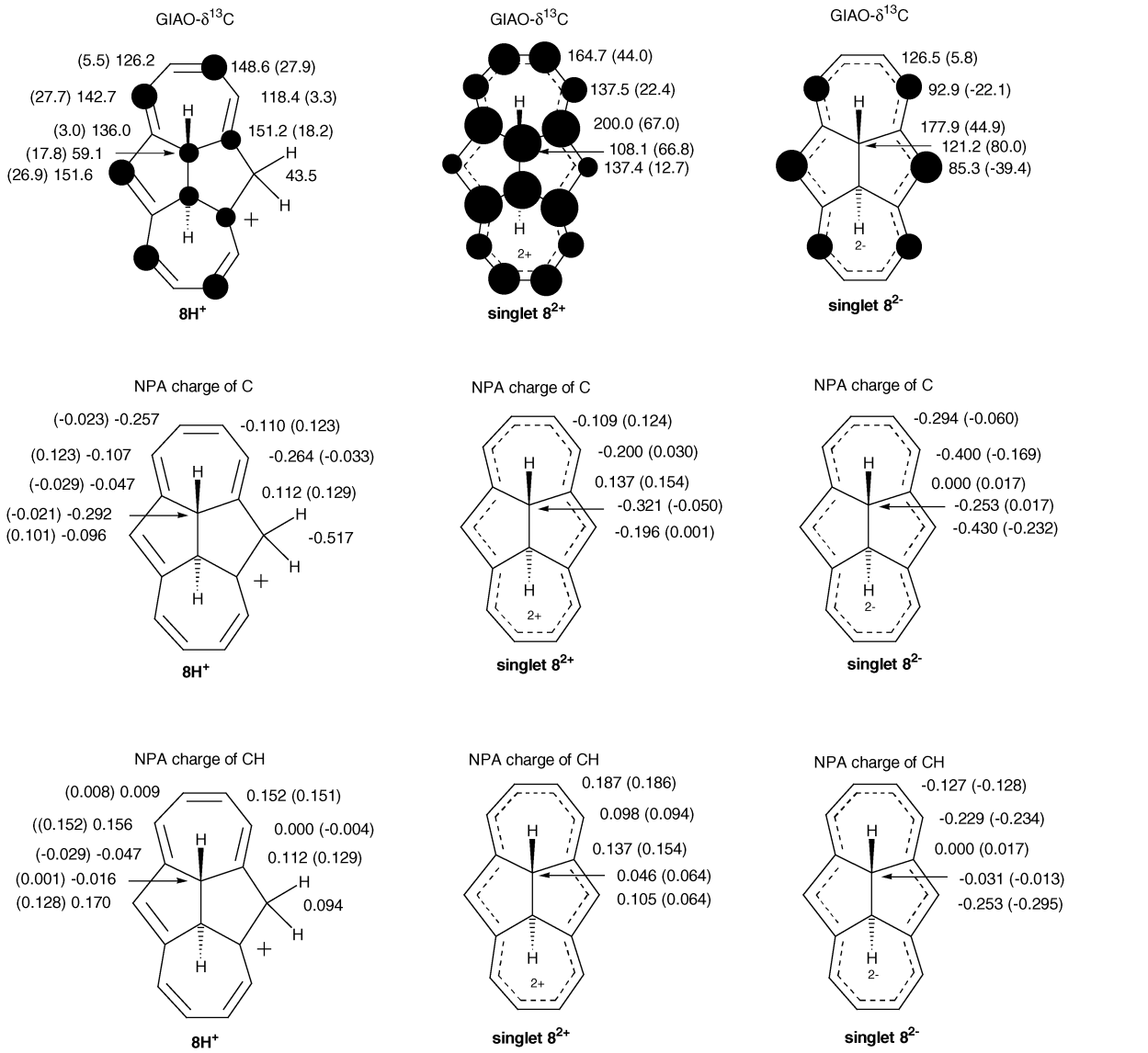

Fig. 8 Computed ^{13}C NMR chemical shifts, NPA-derived carbon charges, and NPA-derived overall charges over CH units for **8**H$^+$, **8**$^{2+}$, and **8**$^{2-}$ ($\Delta\delta$ ^{13}Cs and Δ charges relative to **8** in parentheses). [Dark circles are roughly proportional to the magnitude of $\Delta\delta$ ^{13}Cs (positive/downfield for the carbocations/dication and negative/upfield for the dianion); threshold was set to 10 ppm].

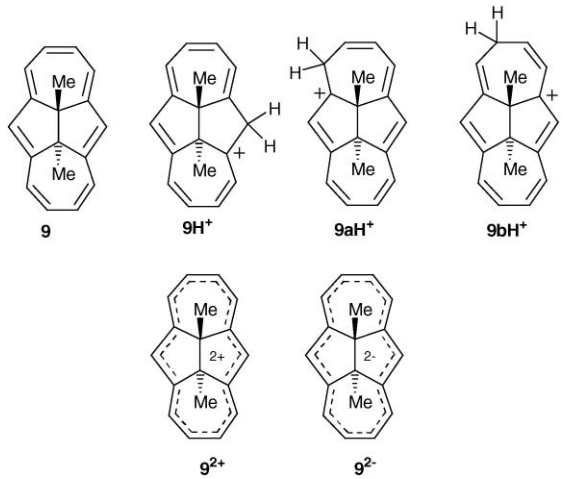

Fig. 9 *trans*-10*b*,10*c*-Dimethyl-10*b*,10*c*-dihydrodicyclohepta[*ed*,*gh*]-pentalene (**9**), annulenium ions (**9**H$^+$, **9a**H$^+$, and **9b**H$^+$), the dication (**9**$^{2+}$), and the dianion (**9**$^{2-}$).

for **11**, the lowest energy monocation is computed to be **11a**H$^+$ (Fig. 12 and Table S2; supplementary information†).

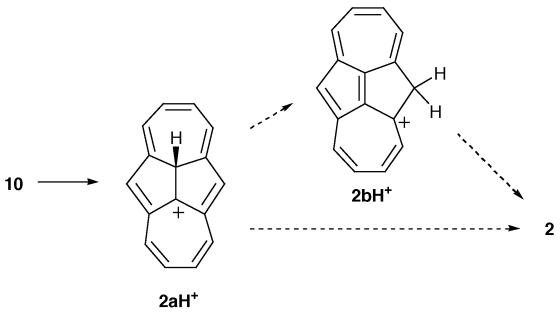

Fig. 10 The mechanism of formation of **2** from **10**.

In comparing the relative carbocation stabilities derived from the *trans*-isomers **8** and **9** with those derived from the *cis*-isomers **10** and **11**, it becomes clear that whereas attack at C-4 is preferred for the former, attack at C-1 is best for the latter.

Noticeable differences in the charge delocalization patterns are computed between the *trans*-carbocations (**8**H$^+$ and **10a**H$^+$) and the *cis*-carbocations (**9**H$^+$ and **11a**H$^+$) (Fig. 8, S8, S13, and S14; supplementary information†), showing that the positive charge is more extensively delocalized in the *trans*-isomers. This is also true in the singlet dications which are more delocalized in

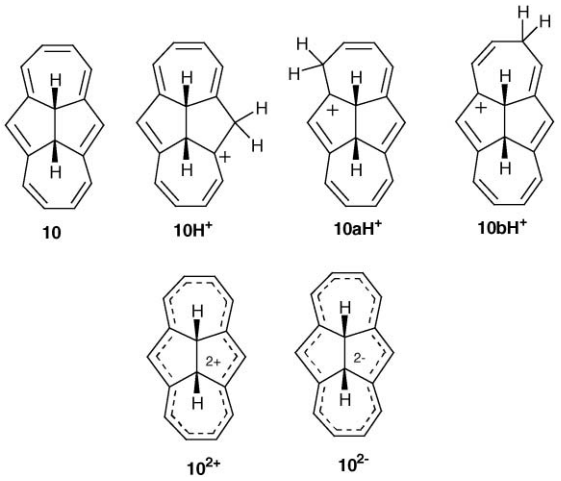

Fig. 11 *cis*-10*b*,10*c*-Dihydrodicyclohepta[*ed*,*gh*]pentalene (**10**), their protonated ions (**10**H$^+$, **10a**H$^+$, and **10b**H$^+$), the dication (**10**$^{2+}$), and the dianion (**10**$^{2-}$).

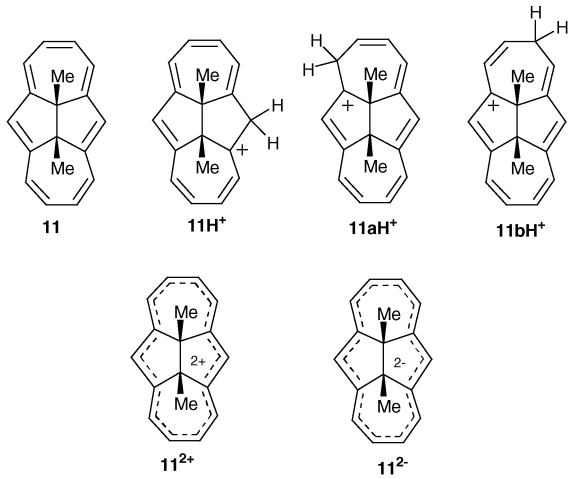

Fig. 12 *cis*-10*b*,10*c*-Dimethyl-10*b*,10*c*-dihydrodicyclohepta[*ed*,*gh*]pentalene (**11**), their protonated ions (**11**H$^+$, **11a**H$^+$, and **11b**H$^+$), the dication (**11**$^{2+}$), and the dianion (**11**$^{2-}$).

the *trans*-isomers. However, the charge patterns in the dianions are similar in both *cis*- and *trans*-annulenes.

Whereas the computed bond lengths in **8**$^{2+}$ and **10**$^{2+}$ are rather close, their differences are larger than the differences in the dianions (**8**$^{2-}$ *versus* **10**$^{2-}$) in particular relative to the central bond which is much longer in the *cis*-isomer (**10**$^{2-}$) (Fig. S6 and S11; supplementary information†).

The singlet **10**$^{2+}$ is only slightly preferred over the triplet (by 1 kcal mol^{-1}), but the singlet **10**$^{2-}$ is computed to be strongly preferred relative to the triplet (by 11 kcal mol^{-1}). The situation for **11** is similar and the singlet **11**$^{2-}$ and singlet **11**$^{2+}$ are both preferred over the triplet states (Table S2, supplementary information†). Fig. S13a provides a basis set dependency study of GIAO chemical shifts for **10a**H$^+$, showing closer correspondence at higher basis sets (see also Fig. S24; supplementary information†).

Charge delocalization modes deduced based on magnitude of GIAO $\Delta\delta^{13}$C values in the monocations **10**H$^+$ and **11**H$^+$, singlet dications **10**$^{2+}$ and **11**$^{2+}$, and singlet dianions **10**$^{2-}$ and **11**$^{2-}$ are sketched in Fig. S13 and S14 for comparison (supplementary information†). The NPA-derived carbon and CH charges and changes in charges are also included.

The computed NICS and ΔNICS values for the dications and dianions derived from **10** and **11** are gathered in Fig. S15 and S16 for comparison (supplementary information†). The singlet dications **10**$^{2+}$ and **11**$^{2+}$are antiaromatic in individual rings and at the center of the annulene. The triplet **10**$^{2+}$ is also antiaromatic in individual rings and at the center, but the triplet **11**$^{2+}$ is computed to be aromatic (in individual rings and in center), and triplet **11**$^{2-}$ is also aromatic.

Protonation, oxidation and reduction of the related bridged [14]annulenes 14 and 15

Structures of **14** (C_1), **14**H$^+$ (C_1), singlet dication **14**$^{2+-}$ (C_1), singlet dianion **14**$^{2-}$ (C_1), **15** (C_1), **15**H$^+$ (C_1), singlet dication **15**$^{2+}$ (C_1), and singlet dianion **15**$^{2-}$ (C_1) were calculated to be minima. These geometries are almost the same as the C_{2v} symmetrical structure for **14**, **14**$^{2+}$, **14**$^{2-}$, **15**, **15**$^{2+}$, and **15**$^{2-}$ (Fig. 13 and 14 and Table S2; supplementary information†)

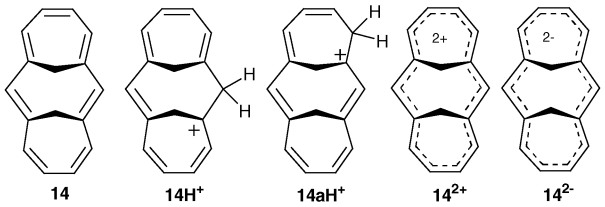

Fig. 13 The bismethano[14]annulene (**14**), its monoprotonated annulenium ions (**14**H$^+$ and **14a**H$^+$), the dication (**14**$^{2+}$), and the dianion (**14**$^{2-}$).

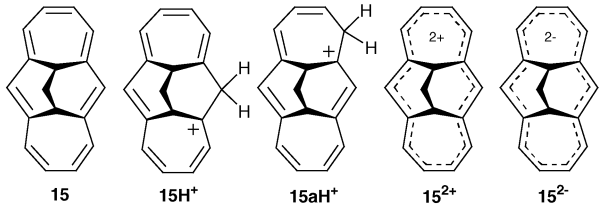

Fig. 14 The propanediylidene[14]annulene (**15**), its monoprotonated annulenium ions (**15**H$^+$ and **8a**H$^+$), the dication (**15**$^{2+}$), and the dianion (**15**$^{2-}$).

Optimized geometries of the annulenium cations, and their dications and dianions are sketched in Fig. S17 and Fig. S18 for comparison (supplementary information†). The X-ray geometries of **14**[27] and **15**[28] are included for comparison with DFT-optimized geometries. Computed bond lengths in parent **14** and **15** are very close to each other and are on average longer than the X-ray derived bond lengths (see also earlier comments on this point). Annulene dications and dianions exhibit strong bond-alternation at their periphery.

Low temperature protonation of **14** initially gave **14**H$^+$ which was then transformed into **14**$^{2+}$.[22] DFT concurs with the experiment, with **14**H$^+$ computed just 0.5 kcal mol^{-1} lower in energy as compared to **14a**H$^+$ (Fig. 13 and Table S2; supplementary information†).

The resulting annulenium ion exhibits strong anthracenium ion character with positive charge alternating over the periphery (Fig. S19, supplementary information†). Comparison between the GIAO-derived δ^{13}C values and the reported NMR chemical shifts (Fig. S20, supplementary information†) shows reasonable overall agreement, except that GIAO strongly underestimates the chemical shifts of C-1/C-13 (using Vogel's numbering system) and one of the sp^3 carbons at the ethano-bridge.

A basis-set dependency study of the GIAO shifts for **14**H$^+$ (Fig. S20, supplementary information†) illustrated that the correspondence between experimental and computed shifts improved somewhat at higher basis sets, but did not produce a perfect fit (see also Fig. S24, supplementary information†). However, the overall charge delocalization pattern (based on magnitude of $\Delta\delta^{13}$C values) is well reproduced

Based on DFT, the singlet **14**$^{2+}$ and singlet **14**$^{2-}$ dianion are strongly preferred relative to their triplet states (Table S2, supplementary information†). Based on the GIAO-derived $\Delta\delta^{13}$C values the singlet **14**$^{2+}$ is extensively charge delocalized with larger

localization of positive charge at the 1,6,8,18-carbons (Vogel numbering system). The negative charge in the dianion is heavily localized at 7,14-carbons and at 2,5-carbons. Consideration of the NPA-derived changes of charges generates essentially the same patterns as GIAO (Fig. S19, supplementary information†).

The NMR data for $\mathbf{14}^{2+}$ and $\mathbf{14}^{2-}$ are reported in the literature[20–22], and enable a direct comparison with GIAO. The outcome of a basis set dependency study of the computed shifts *versus* experiment is illustrated in Fig. S21a–c (supplementary information†) showing some variation as a function of basis set and very good overall correspondence (specially for the dianion) (see also Fig. S24, supplementary information†).

Low temperature protonation of **15** gave $\mathbf{15}H^+$ as the NMR observable species, which on increasing temperature, was transformed into $\mathbf{15}^{2+}$.[22] According to DFT, annulenium ion $\mathbf{15a}H^+$ is actually 3.7 kcal mol^{-1} lower in energy relative to the observed $\mathbf{15}H^+$. The GIAO-derived charge delocalization maps for $\mathbf{15}H^+$ and $\mathbf{15a}H^+$ are illustrated in Fig. S22 for comparison (for basis-set dependency of GIAO shifts in comparison to experiment see Fig. S22a,b and Fig. S24; supplementary information†). It can be seen that charge delocalization patterns in $\mathbf{14}H^+$ and $\mathbf{15}H^+$ are rather similar (*i.e.* transforming the bis-methano-bridge to the propanediylidene unit does not induce a significant effect in charge delocalization at the periphery of the annulenium ions), but that for $\mathbf{15a}H^+$ is quite different.

The ^{13}C NMR data for $\mathbf{15}^{2+}$, reported independently by Müllen *et al.*[21] *via* oxidation in SbF_5/SO_2ClF, and by Michl and associates[22] *via in situ* formation upon warming the FSO_3H solution of $\mathbf{15}H^+$, show rather noticeable medium effect on chemical shifts. The ^{13}C NMR data for $\mathbf{15}^{2-}$ do not appear to exist in the literature (only the ^{1}H NMR data for the dianion are reported in ref. 21).

GIAO-derived charge delocalization maps for singlet $\mathbf{15}^{2+}$ and singlet $\mathbf{15}^{2-}$ are included in Fig. S22 for comparison (for basis-set dependency of GIAO shifts in comparison to experiment see Fig. S22d,e and Fig. S24; supplementary information†). These may be compared with the charge pattern for singlet $\mathbf{14}^{2+}$ and singlet $\mathbf{14}^{2-}$ (in Fig. S19; supplementary information†). Whereas there are differences in the magnitude of $\Delta\delta^{13}$C values, the overall delocalization patterns are similar. It is noteworthy that in singlet $\mathbf{15}^{2+}$ not only the peripheral carbons but also the bridge carbon (C_{10c}; C_{16}) become positive.

Finally, the computed NICS and ΔNICS values measured at the center for the annulene dications and dianions from **14** and **15** are gathered in Fig. S23 (supplementary information†). NICS values for the singlet and triplet $\mathbf{14}^{2-}$ and singlet $\mathbf{15}^{2-}$ were also computed at higher basis set. For both types of bridged annulenes, the singlet dications and dianions are antiaromatic at the center, but the triplet dications and triplet dianions are predicted to be aromatic.

Comparative discussion and summary

The present DFT study has examined the annulenium ions of protonation, annulene dications and dianions derived from several *cis*- and *trans*-dihydro derivatives of the nonalternant isomers of pyrene namely azupyrene **1** and dihydro-dicyclohepta[*ed*,*gh*]pentalene **2**. Whereas the *trans*-dihydro derivatives of **1** (*i.e.* **4** and **5**) are more stable than *cis* (*i.e.* **6** and **7**), the *cis* isomers are strongly preferred in the case of **2** (**10** and **11** are far better than **8** and **9**). Since **10** and **11** belong to the family of [14]bridged annulenes, two representative cases (**14** and **15**) were included in this investigation. Geometrical features, GIAO NMR shifts, NPA charges and NICS have been examined.

For **4** and **5** protonation at C-4 is most favored and the resulting annulenium monocations are extensively delocalized. The singlet and triplet dications and dianions derived from **4** and **5** are all minima, with the triplet dication and singlet dianion being more stable (except at the B3LYP/6–31++G(d,p) level where triplet $\mathbf{4}^{2-}$ was computed to be more stable than singlet $\mathbf{4}^{2-}$). The C_4/C_9 sites in the dianions exhibit the largest localization of negative charge.

For *trans*-dihydro derivatives **8** and **9**, protonation at the 5-membered ring is most favored resulting in highly delocalized annulenium ions. The singlet and triplet dications and dianions derived from **8** and **9** were all computed to be minima, with the singlet states having lower energies. Positive charges in the singlet dications are delocalized over the entire periphery and on the central bond, whereas negative charges in the dianions are more localized, with the largest $\Delta\delta^{13}$C upfield shifts at C_5/C_{10} carbons.

The lowest energy annulenium cation derived from **10** and **11** (both *cis*) is formed by protonation at C-1 and this is in concert with experimental observation of $\mathbf{10a}H^+$ in superacid media.[22] The resulting annulenium ions are less delocalized than those *via* **8** and **9**.

DFT and stable ion study are also in concert regarding the protonation of **14**. The availability of X-ray structures and stable ion NMR data for the dications and dianions of **14** and **15** enabled comparison with the DFT-optimized structures and GIAO NMR shifts.

Inclusion of diffuse functions in the basis sets generally resulted in lowering of the energies which was more pronounced for the dianions (both singlet and triplet) (Table S2–S4, supplementary information†). The computed NICS(0) values suggested that in most cases the triplet dications and triplet dianions are aromatic and the singlet dications and singlet dianions have antiaromatic character, despite the fact that the singlet dications and singlet dianions are lower in energy than their corresponding triplet states.

Acknowledgements

This work was supported in part by the NCI of NIH (NCI 2 R15 CA07835-02A1), by a grant in Aid for Young Scientists (B) 15710160 from the Japan Society for the Promotion of Science (JSPS), and by 21st century COE program, COE for United Approach to New Materials Science (COE program of the Ministry of Education, Culture, Sports, Science and Technology, Japan).

References

1 E. Vogel, H. Wieland, L. Schmalstieg and J. Lex, *Angew. Chem., Int. Ed. Engl.*, 1984, **23**, 717.
2 A. G. Anderson, Jr., S. C. Critchlow, L. C. Andrews and R. D. Haddock, *Acta. Crystallogr., Sect. C*, 1990, **C46**, 439.
3 (*a*) A. G. Anderson Jr., A. A. McDonald and A. F. Montana, *J. Am. Chem. Soc.*, 1968, **90**, 2993; (*b*) A. G. Anderson Jr., A. F. Montana and A. A. McDonald, *J. Org. Chem.*, 1973, **38**, 1445; (*c*) A. G. Anderson Jr., G. M. Masada and A. F. Montana, *J. Org. Chem.*, 1973, **38**, 1439; (*d*) A. G. Anderson Jr., E. R. Davidson, E. D. Daugs, L. G. Kao, R. L. Lindquist and K. A. Quenemoen, *J. Am. Chem. Soc.*, 1985, **107**, 1896.
4 Progress Review: A. G. Anderson, Jr., *Trends Org. Chem.*, 1992, **3**, 315.
5 H. Reel and E. Vogel, *Angew. Chem., Int. Ed. Engl.*, 1972, **11**, 1013.
6 C. J. Jutz and E. Schweiger, *Synthesis*, 1974, 193.
7 K. Hafner, H. Diehl and W. Richarz, *Angew. Chem.*, 1976, **4**, 125.
8 T. Okazaki and K. K. Laali, *Org. Biomol. Chem.*, 2004, **2**(15), 2214.
9 V. Boekelheide and J. B. Phillips, *J. Am. Chem. Soc.*, 1967, **89**, 1695.
10 (*a*) R. H. Mitchell, R. J. Carruthers, L. Mazuch and T. W. J. Dingle, *J. Am. Chem. Soc.*, 1982, **104**, 2544; (*b*) R. H. Mitchell, R. V. Williams and T. W. Dingle, *J. Am. Chem. Soc.*, 1982, **104**, 2560; (*c*) R. H. Mitchell, R. V. Williams, R. Mahadevan, Y.-H. Lai and T. W. Dingle, *J. Am. Chem. Soc.*, 1982, **104**, 2571; (*d*) R. H. Mitchell, J. S. H. Yan and T. W. Dingle, *J. Am. Chem. Soc.*, 1982, **104**, 2551.
11 (*a*) Y.-H. Lai, P. Chen and T.-G. Peck, *Pure Appl. Chem.*, 1993, **65**, 81; (*b*) Y.-H. Lai, P. Chen and T. W. Dingle, *J. Org. Chem.*, 1997, **62**, 916.
12 (*a*) R. H. Mitchell, Y. S. Iyer, M. Khalifa, R. Mahadevan, S. Venugopalan, S. Weerawarna and P. J. Zhou, *J. Am. Chem. Soc.*, 1995, **117**, 1514; (*b*) R. H. Mitchell and D. Y. K. Lau, *Tetrahedron Lett.*, 1995, **36**, 9281.

13 (*a*) J. B. Phillips, R. J. Molyneux, E. Sturm and V. J. Boekelheide, *J. Am. Chem. Soc.*, 1967, **89**, 1704; (*b*) Y.-H. Lai and J. J. Jiang, *J. Org. Chem.*, 1979, **44**, 4733; (*c*) R. H. Mitchell, in *Advances in Theoretically Interesting Molecules*, ed. B. Halton, JAI Press, Stamford, CT, 1989, vol. 1, p 135.
14 R. H. Mitchell, C. E. Klopfenstein and V. Boekelheide, *J. Am. Chem. Soc.*, 1969, **91**, 4931.
15 K. K. Laali, S. Bolvig, T. J. Raeker and R. H. Mitchell, *J. Chem. Soc., Perkin. Trans. 2*, 1996, 2635.
16 K. K. Laali, M. Tanaka, R. H. Mitchell and D. Y. K. Lau, *J. Org. Chem.*, 1998, **63**, 3059.
17 K. K. Laali, T. Okazaki, R. H. Mitchell and T. R. Ward, *J. Org. Chem.*, 2001, **66**, 5329.
18 R. H. Mitchell, Y. Chen, V. S. Iyer, D. Y. K. Lau, K. K. Baldrige and J. S. Siegel, *J. Am. Chem. Soc.*, 1996, **118**, 2907.
19 (*a*) J. Alexander, M. Baumgarten, K.-U. Klabunde and K. Müllen, *Tetrahedron Lett.*, 1991, **32**, 735; (*b*) K. Müllen, *Pure Appl. Chem.*, 1986, **58**, 177.
20 K. Müllen, *Chem. Rev.*, 1984, **84**, 603.
21 K. Müllen, T. Meul, P. Schade, H. Schmickler and E. Vogel, *J. Am. Chem. Soc.*, 1987, **109**, 4992.
22 G. M. Wallraff, E. Vogel and J. Michl, *J. Org. Chem.*, 1988, **53**, 5807–5812.
23 *Gaussian 03, Revision B.05*, M. J. Frisch, G. W. Trucks, H. B. Schlegel, G. E. Scuseria, M. A. Robb, J. R. Cheeseman, J. A. Montgomery, Jr., T. Vreven, K. N. Kudin, J. C. Burant, J. M. Millam, S. S. Iyengar, J. Tomasi, V. Barone, B. Mennucci, M. Cossi, G. Scalmani, N. Rega, G. A. Petersson, H. Nakatsuji, M. Hada, M. Ehara, K. Toyota, R. Fukuda, J. Hasegawa, M. Ishida, T. Nakajima, Y. Honda, O. Kitao, H. Nakai, M. Klene, X. Li, J. E. Knox, H. P. Hratchian, J. B. Cross, C. Adamo, J. Jaramillo, R. Gomperts, R. E. Stratmann, O. Yazyev, A. J. Austin, R. Cammi, C. Pomelli, J. W. Ochterski, P. Y. Ayala, K. Morokuma, G. A. Voth, P. Salvador, J. J. Dannenberg, V. G. Zakrzewski, S. Dapprich, A. D. Daniels, M. C. Strain, O. Farkas, D. K. Malick, A. D. Rabuck, K. Raghavachari, J. B. Foresman, J. V. Ortiz, Q. Cui, A. G. Baboul, S. Clifford, J. Cioslowski, B. B. Stefanov, G. Liu, A. Liashenko, P. Piskorz, I. Komaromi, R. L. Martin, D. J. Fox, T. Keith, M. A. Al-Laham, C. Y. Peng, A. Nanayakkara, M. Challacombe, P. M. W. Gill, B. Johnson, W. Chen, M. W. Wong, C. Gonzalez, and J. A. Pople, Gaussian Inc., Pittsburgh PA, 2003.
24 (*a*) P. v. R. Schleyer, C. Maerker, A. Dransfeld, H. Jiao and J. v. E. Hommes, *J. Am. Chem. Soc.*, 1996, **118**, 6317; (*b*) N. S. Mills, *J. Am. Chem. Soc.*, 1999, **121**, 11690; (*c*) A. Levy, A. Rakowitz and N. S. Mills, *J. Org. Chem.*, 2003, **68**, 3990; (*d*) N. S. Mills, *J. Org. Chem.*, 2002, **67**, 7029; (*e*) I. Alkorta, I. Rozas and J. Elguero, *Tetrahedron*, 2001, **57**, 6043.
25 (*a*) K. Wolinski, J. F. Hinton and P. Pulay, *J. Am. Chem. Soc.*, 1990, **112**, 8251; (*b*) R. Dichfield, *Mol. Phys.*, 1974, **27**, 789.
26 R. Bianchi, G. Gasalone and M. Simonetta, *Acta Crystallogr., Sect. B*, 1975, **B31**, 1207.
27 R. Destro, T. Pilati and M. Simonetta, *Acta Crystallogr., Sect. B.*, 1977, **B33**, 940.
28 A. Gavezzotti, A. Mugnoli, M. Raimondi and M. Simonetta, *J. Chem. Soc., Perkin Trans. 2*, 1972, 425.